Acta Geologica Sinica (English Edition), 2021, 95(2): 558–569

Pore Structure Characterization of Clay Minerals in the Lower Karamay Formation Conglomerate Reservoir in the Junggar Basin and its Impact on Hydrocarbon Storage and Seepage

Taskyn ABITKAZY[1, 2], DU Shuheng[3, *], XU Feng[2] and SHI Yongmin[1]

[1] *School of Earth and Space Sciences, Peking University, Beijing 100871, China*
[2] *Research Institute of Petroleum Exploration and Development Co., Ltd., CNPC, Beijing 100083, China*
[3] *State Key Laboratory of Nonlinear Mechanics, Institute of Mechanics, Chinese Academy of Sciences, Beijing 100190, China*

Abstract: The micro-nano pore structure of conglomerate in the Lower Karamay Formation of the Xinjiang Oilfield, Junggar Basin, northern China is characterized to predict its impact on fluid reserves and seepage. Authigenic clay minerals are mainly kaolinite (67%), followed by an illite/smectite mixed layer (18%), illite (10%), and chlorite (5%). For kaolinite, pore throats between 0–200 nm are dominant, accounting for 90% of the total pore throats. For illite/smectite mixed layer, pore throats also between 0–200 nm account for nearly 80%, while pore throats between 200-500 nm only account for 15%. For illite, pore throats below 100 nm account for about 80%, while pore throats in the range of 100–500 nm only account for 20%. For chlorite, most throats are below 200 nm. The pore roundness of illite is the highest, while the pore roundness of chlorite is relatively lower. The lower limits of the dynamic and static pore throat radii are 42.128 nm and 72.42 nm, respectively. The theoretical contribution rates of the illite/smectite mixed layer, kaolinite, illite and chlorite to storage/seepage are 60%/45.86%, 52.72%/38.18%, 37.07%/28.78% and 32.97%/26.3%, respectively. Therefore, the contribution rates of clay minerals in the study area are as follows: illite/smectite mixed layer, kaolinite, illite and chlorite.

Key words: oil, conglomerate, clay minerals, micro-nano pore, reservoir characterization, Triassic, Xinjiang

Citation: Abitkazy et al., 2021. Pore Structure Characterization of Clay Minerals in the Lower Karamay Formation Conglomerate Reservoir in the Junggar Basin and its Impact on Hydrocarbon Storage and Seepage. Acta Geologica Sinica (English Edition), 95(2): 558–569. DOI: 10.1111/1755-6724.13887

1 Introduction

Composed of typical continental clastic rocks, a conglomerate reservoir is an important reservoir type within China's continental hydrocarbon resources. Regarding conglomerate reservoirs, the important elements are rock skeletons, pores and fluids in pores. When flooding affects a developed oilfield over a long time, some of the soluble components in the crude oil can be taken away by groundwater as water washes the oil layer during the flow process, whereas many insoluble components and macromolecular aromatic hydrocarbons remain in the strata. As a consequence, the mineral particles are surrounded by a complex environment mixed with oil and water (Su et al., 2007; Sakthivel et al., 2012; Liu et al., 2017; Mohammadi et al., 2021). The environment is mainly composed of interstitial materials, matrix and cement, and other foreign objects, and a relatively active interface layer with a thickness of 30–60 μm is formed between the particles and the pores. The interface layer largely determines the physical and chemical properties of the reservoir, restricts the distribution of movable oil, movable water, bound oil and bound water, and ultimately greatly affects the recovery ratio.

In recent years, much fruitful research has been done on the pore throat, configuration of conglomerate reservoirs and its significance to reservoir and permeability. From a macroscopic viewpoint, the main controlling factors of conglomerate reservoirs are sedimentary facies (Arnott, 2003; Clifton, 2003; Hart and Plint, 2003; Rogers, 2007; Jia et al., 2017), diagenesis (Salem et al., 2000; Morad et al., 2010; Taylor et al., 2010; Carvalho and Ros, 2015; Wei et al., 2015; Mahmic et al., 2018) and tectonic movements (Rogers, 2007). From a microscopic viewpoint, the main controlling factors are matrix type and filling mode (Arnott, 2003; Rogers, 2007; Jia et al., 2017), and grain size distribution (Liu et al., 2012; Jia et al., 2017).

Hurst (1999) quantified the micro-pores of clastic reservoirs using backscattered electron images of clay minerals and found that fibrous clay minerals are developed with many micro-pores. Cerepi et al. (2002) quantified the microscopic geometry of pores from submicron to millimeter scale through petrographic image analysis of sandstone reservoirs, and through these geometric parameters, they studied the feasibility of modeling reservoir properties. Kuila et al. (2014) studied the air at nano-scale by X-ray diffraction and pyrolysis adsorption, taking the unconventional rock samples in the

* Corresponding author. E-mail: dushuheng@imech.ac.cn

Baltic Sea Basin and different regions as examples. The results show that nano-scale micro-pores in mudstone are mainly composed of network-like micro-pores and meso-pores in clay minerals. In addition, some scholars have researched many nano-pores between clay particles and at the internal cracking surface of the clay particles in unconventional oil and gas reservoirs (Nelson, 2009; Curtis et al., 2012; Yao et al., 2012). The contribution of the configuration of clay minerals to reservoirs has also been studied (Chen et al., 2016).

Clarke (1979) first conducted a mathematical analysis and described the characteristic curves of conglomerate and granular sandstone reservoir configuration, and then proposed the concept of a bimodal structure of conglomerate and established the expression of porosity and permeability of rocks with bimodal structure. Liu (1983) first proposed the concept of a multimodal structure through the complex structure of the reservoir in the Karamay oilfield, NW Junggar and explained that the modal structure of the reservoir is the theoretical model of the reservoir pore configuration from the microscopic view. Luo (1992) called this structure a three-mode structure, and divided the three-mode mechanism into three-mode suspension and three-mode filling according to the content of secondary or tertiary particles.

More recent research has focussed on the microscopic characteristics of reservoirs such as petrological characteristics, physical properties, seepage characteristics and pore configuration (Song et al., 2007, 2009; Lv et al., 2015; Zhang et al., 2013; Yin et al., 2018; Xiao et al., 2019). Through rate-controlled mercury penetration, casting thin sections and other means, such studies have qualitatively and quantitatively evaluated the shape and size of the pore throat and the characteristics of connectivity, and concluded that the higher the heterogeneity of the pore throat structure, the lower the water flooding efficiency. During water flooding, the displacement morphology and motion mode are different in large and small throats: flow in large throats moves forward as slug flow; with decreasing throat size, the motion morphology changes to fingering and water channelling. The difference in physical properties and microscopic pore configuration lead to the differences in the mechanism of microscopic oil displacement (water flooding or chemical flooding).

The lithofacies of piedmont alluvial fan deposits change rapidly, the reservoir heterogeneity is strong, and the clay mineral content changes rapidly with depth. The content, composition, and occurrence of interstitial materials have a great impact on the development of glutenite oilfields (Feng et al., 2019; Li et al., 2020; Yang et al., 2020). The distribution of clay minerals on the pore channel wall of the reservoir and in the middle of pores makes the pore channel of the reservoir rock more complicated. If clay minerals loosely combine with the skeleton particles, it is easy to block the pore throat when physical migration happens under the high flow velocity of the invading fluid. For example, flake illite, scattered kaolinite and chlorite have pores divided into numerous micropores, which makes the pore throat become circuitous and reduces the reservoir physical properties (Li et al., 2017) In an oilfield storage with nano-scale pores, the occurrence and ultimate availability of oil and gas are the most important scientific issues for exploration and production (Zou et al., 2011; Hu et al., 2020).

In this paper, samples of the Triassic Lower Karamay Formation (Fm.) of the Junggar Basin were selected to conduct a series of experiments. The morphological characteristics of the clay minerals were determined from a large number of rock thin sections, scanning electron microscopy and other experimental methods. The clay mineral compositions of the rocks were determined by XRD diffraction. A large number of morphological characterization parameters were selected to finely characterize the pore throat development characteristics of the main clay mineral types. Then, by introducing the relevant dynamic and static pore throat lower limit model, combined with a specific surface test—the irreducible water saturation test and the high-pressure mercury intrusion test—the lower limits of the dynamic and static pore throat radius of conglomerate in the Lower Karamay Fm. were calculated. The aim is to determine the storage and seepage contribution rates of clay minerals in conglomerate reservoirs to clarify their significance to storage and seepage.

2 Geological Setting

The study area is a block in the Xinjiang Oilfield on the northwestern edge of the Junggar Basin in northwestern China (Fig. 1a). The Triassic Lower Karamay Fm. is the main production layer, which unconformably overlies Carboniferous strata with piedmont-alluvial deposits (Liu, 1983; He et al., 2014; Lv et al., 2015). The depth of the formation ranges from 1100 m to1400 m and divided into S6 and S7 two sets (sand groups) and more beds (sand strata). The S7 layers are composed of thick gravel-sandstone, conglomerate and mudstone interbedded to fine siltstone-mudstone. Layers of S6 are alternately composed of gravel and mudstone (Zhang et al., 2013; He et al., 2014; Yin et al., 2018: Fig. 1b). Because of factors such as sedimentation, tectonism, diagenesis and fluid modification in the later stage, the Lower Karamay Fm. conglomerate reservoir is characterized by strong heterogeneity, poor connectivity, and rapid variation, etc. The sedimentation of the Triassic piedmont-alluvial fan has determined the microscopic characteristics of the composition and size, the matrix components and content, and the rock fabrics (gradation, roundness, supporting form, etc.) of the conglomerate particles. Lithologies control the reservoir physical properties. Compaction, cementation, dissolution, and recrystallization during the later diagenetic stage led to the development of a multimodal pore structure with weak pore connectivity, poor pore configuration and physical properties, and argillaceous fillers in the pores and pore throats (Lai et al., 2013; Rong et al., 2014; Pan et al., 2019; Rafiei et al., 2019).

3 Methods

3.1 X-Ray diffraction

XRD was used to analyse materials and their diffraction

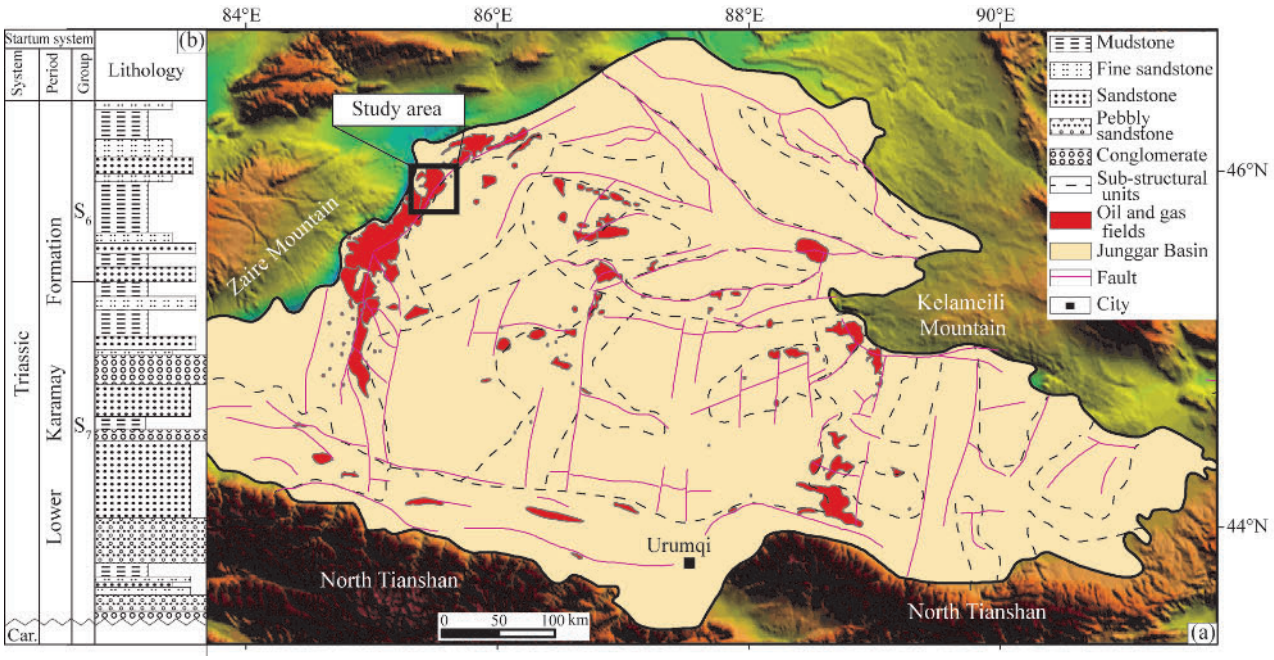

Fig. 1. Location of (a) the study area and (b) lithology of the Lower Karamay Formation (b from Yin et al., 2018).

patterns and to obtain information about material composition, atomic or molecular structure, and the form of materials. When a substance (crystal or amorphous) is analyzed by diffraction, it is irradiated by the X-ray to produce different degrees of diffraction. The material composition, crystal form, intramolecular bonding mode, molecular configuration, and conformation determine the specific diffraction pattern of the material. There are many advantages of XRD: ① the sample is not damaged; ② it is pollution-free and fast; ③ it has high measuring precision; and ④ it obtains complete information about crystal integrity. We used this method to investigate material phase and crystal structure.

3.2 Feil emission scanning electron microscopy (FE-SEM) and energy dispersive spectroscopy (EDS)

The working principle of imaging is that the electron gun generates a certain energy emission current according to the magnitude of the acceleration voltage, the electron beam intensity and beam spot size are controlled by focusing the electromagnetic lens, and the far-axis electrons are filtered by changing the aperture of the objective lens to form a steady fine probe current and beam spot, and to scan the surface of the sample point by point. The instrument used was the QUANTA-650FEG Sputter Coaters and SEM/TEM Carbon Coaters (Q150T ES (QUANTA-650FEG Sputter Coaters and SEM/TEM Carbon Coaters (Q150TES) system (FEI Company of USA), a multifunctional field emission scanning electron microscope with high resolution static and dynamic observation and analysis. The EDS instrument used is a X-Max5 model (Oxford Instruments, UK). The trace element spectrometer (Inca synergy model, Oxford Instruments) can simultaneously perform qualitative, semi-quantitative, and quantitative analysis on the surface of the sample, along with comprehensive analysis of topography and chemical composition, and can analyze the particle minimum size of 40–50 nm.

The test process was as follows: firstly, a sheet was cleaned with alcohol and blown dry, then it was put into the coating apparatus to gain a chromium conductive layer of 5 nm. The test distance is 10–11 mm, the voltage is 10 kV, SPOT and APE are 5.

3.3 Image processing

The high-resolution image processing method can directly provide the two-dimensional shape of the pore throat, which is much closer to the real shape, even recognizing nanometer level (minimum 20 nm). Firstly, the pore throat and particle are distinguished by comparing the results of BSE image and EDS element analysis, and then the appropriate gray scale selected by the high-resolution image processing method is used to segment the image and calculate the pore parameters. All the pores are separated out, and the individual pore throat is extracted. The individual pore throat parameters including such as Area, Circularity, Solidity, Major and Minor (Zeng et al., 2020). Major and Minor are the primary and secondary axes of the best fitting ellipse. Circularity is same as shape factor, but in the formula of these two parameters, Circularity has a term of 4π more than shape factor, which is in order to increase the relative value of the Circularity (1):

where, S, area of the pore throat, μm^2; C, perimeter of the pore throat, μm^2.

$$\text{Circularity} = 4\pi \cdot \frac{S}{C^2} \tag{1}$$

Solidity is a value of 0 to1; as the value approaches 1, it indicates a perfect circle; as the value approaches 0, it indicates increasing deformation (2):

$$\text{Solidity} = \frac{S}{S_t} \tag{2}$$

where, S, area of the pore throat, μm^2; S_t, the concave and convex area of the pore throat, μm^2.

4 Results

4.1 Grain size analysis and XRD analysis

The grain size analysis and X-ray diffraction analysis show that 18 samples from the Lower Karamay Fm. conglomerate is mainly composed of coarse, medium, and fine conglomerate (64.82%), and is filled with coarse and medium-fine sand and mud (35.18%). The overall rock composition is complex. The particle types of the conglomerate composition in the reservoir rock are mainly granite debris, tuff debris and a little rhyolite debris. The compositions of the different conglomerates are uneven. For example, in the medium-fine sandy conglomerates, the content of granite in the sand composition is 6.75%, whereas the content of granite in the conglomerate composition is up to 48.75% (Fig. 2a–b). Particles in the sandstone are mainly quartz, feldspar and mainly sub-angular to sub-rounded debris with greatly varied grain size, moderate to poor gradation and poor roundness (Zhang et al., 2013; Xie et al., 2017; Liu et al., 2020). Both matrix-supported and particle-supported rocks are found. The skeleton particles are mainly in point contact and line contact with each other, and some of them have been subjected to stronger compaction and appear in line contact.

The sedimentary facies of the reservoir rocks in the study area consists of a rapidly deposited piedmont-alluvial fan, so that the content of the fine-grained interstitial materials deposited with the coarse debris is complex, both in matrix and cement. The matrix is mainly composed of mud and hydromica, which ranges from silt to fine sand in grain size. Matrix particles mostly fill between grains and partly attach to the surface of particles (Fig. 2c), and the crystal form of the particles is poor. Cements include carbonate, sulfate, and pyrite, etc. Carbonate cements are mainly calcite, followed by siderite and ankerite, and they are mostly in small crystals that are euhedral and subhedral. They are mostly in the form of nodular, continuous, and speckled, partially infilling intergranular pores, which easily leads to the compaction of the rocks. Intergranular pores are developed in interstitial materials and debris, and some of their edges suffered corrosion. The interstitial content is inconsistent between different rocks. For example, mud content in a coarse sand-fine gravel interstitial can reach 9.31%, while hydromica in a medium-fine glutenite can reach 2.88% (Fig. 2c). The rock cementation types in the study area are diverse. For medium-fine glutenite, cementations are mainly carbonate minerals, siderite, and anhydrite, whereas, for mélange of sand, conglomerate, and mud, pyrite and other cementation types exist besides carbonate minerals and anhydrite (Fig. 2c–d).

The type and content of minerals and clay minerals of 18 samples of the Lower Karamay Fm. in Tx, Ty and Tz wells in the study area were determined by X-ray diffraction analysis. The average contents of quartz, potassium feldspar, plagioclase, calcite, dolomite, and total clay minerals of the conglomerate reservoir in the study area are 47%, 12%, 24%, 3%, 2%, and 10%, respectively (Fig. 3a). The authigenic clay minerals are mainly kaolinite (67%), followed by an illite/smectite mixed layer (18%), illite (10%), and chlorite (5%) (Fig. 4b).

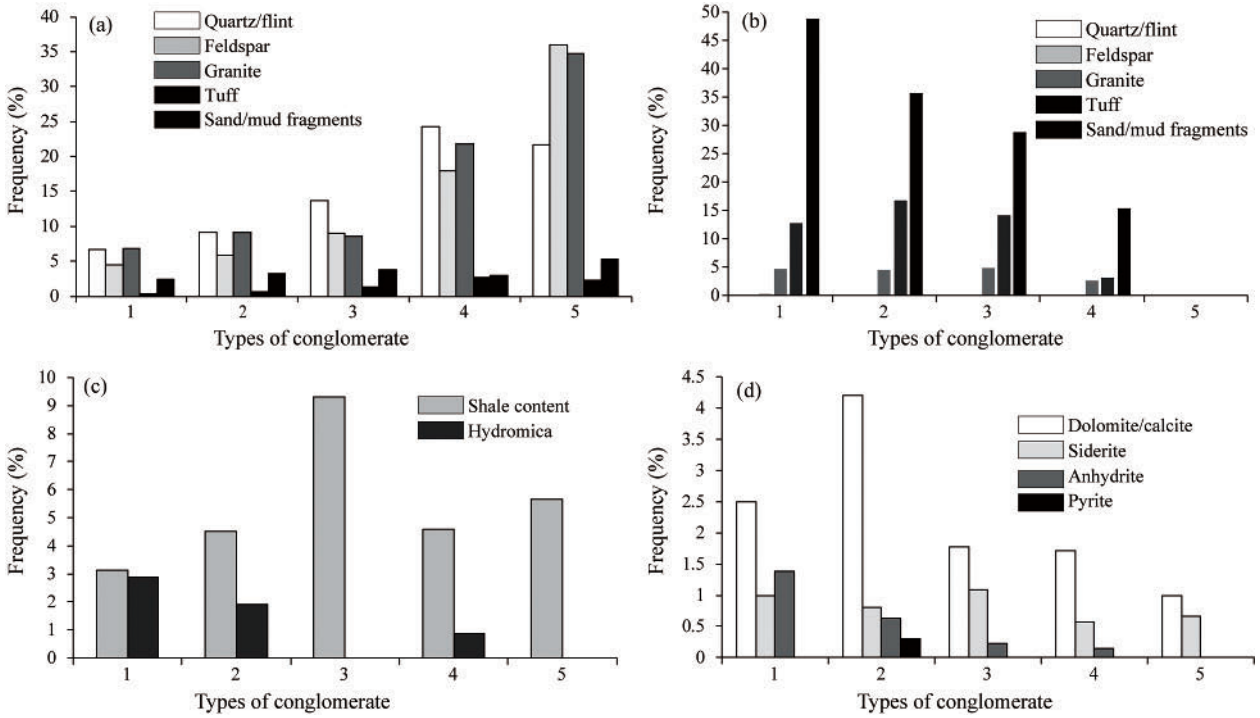

Fig. 2. Graphs of the different lithologic structure component features of the Lower Karamay Formation
(a) Sandy clastic content; (b) gravel particle content; (c) matrix content; (d) cement content; 1, medium-fine sandy conglomerate; 2, gravel mud mélange; 3, grit fine conglomerate; 4, pebbly gritstone; 5, muddy fine siltstone).

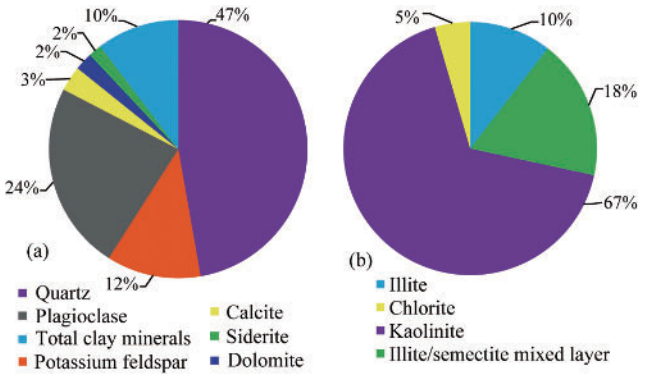

Fig. 3. Pie-diagram analysis of (a) whole rock minerals and (b) relative content of clay minerals.

4.2 FE-SEM characterization and EDS analysis

4.2.1 FE-SEM observation

FE-SEM microscopy showed that kaolinite is the most widely distributed mineral type in the study area. Vermicular and sheet-like kaolinites were observed in almost each sample (Fig. 4a, 4b), and small amounts of kaolinites were observed as dispersed monomers and collections. Moreover, there are precipitations of pyrite crystals on the surface of some kaolinites. Generally, the shale content of the cement is 3%–6%, and the calcite content in the cement is small (3%–4%). The particle arrangement is relatively loose, and the particle surface is relatively clean. The compositional maturity and textural maturity of the reservoir are poor. Feldspar dissolution is common. Pores are relatively developed and contact type

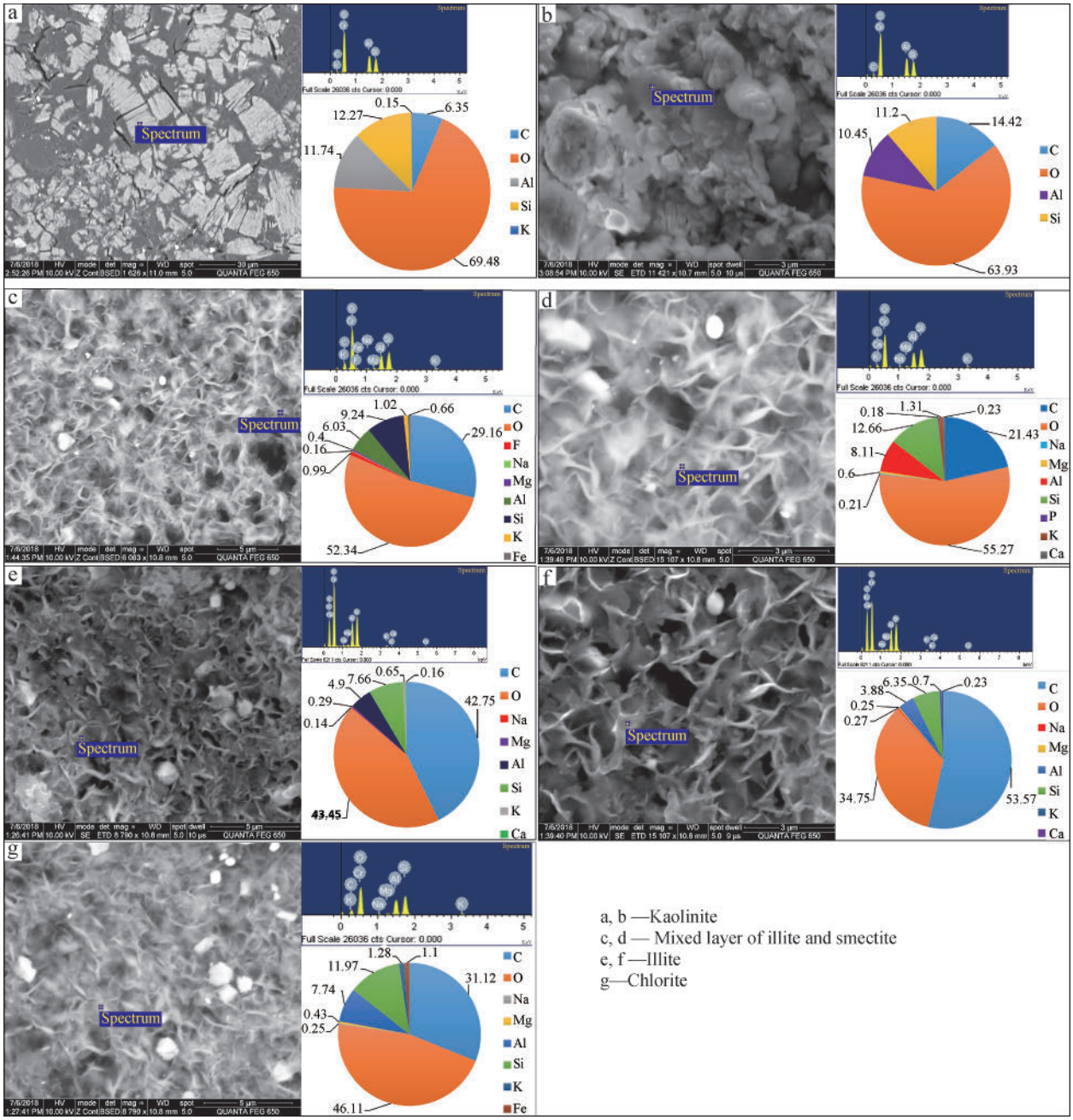

Fig. 4. FE-SEM, EDS and contents of different clay minerals of the study area.

and pore-contact type are the main cementation forms.

Illite/smectite mixed layers are mainly distributed along the surface of the matrix minerals in membrane and honeycomb shapes, with thickness ranging from 50 μm to 157 μm (Fig. 4c–d). The illite/smectite occurring of/in honeycomb, silk-, strip- or bridge-like form extends from the surface of the mineral grains and intersect pore spaces, leading to thinner, smaller and more complex pore throats (Fig. 4). The shale content of the cement is similar to that of the inner lining sandstone, with pores moderately developed, and the quartz secondarily enlarged, resulting in regenerated cementation. In addition, the distribution of fibrous illite in the pores (Fig. 4e–f) changes the original intergranular pores of the conglomerate into small pores between the clay mineral grains. Illite is capable of forming a variety of crystal textures, sometimes existing in pores with irregular fibrous structures. Chlorite has rarely been seen in scanning electron microscopy; it is mainly distributed between the particle aggregates as triangular pores, and there are individual slit-like pores between local plate-like particles (Fig. 4g).

4.2.2 Pore throat distribution of four clay minerals

For different clay minerals, the distribution of the micro-nano pore throat radius has a dominant distribution area, indicating that the pores of the different clay minerals have different effects on the storage and seepage of oil. For kaolinite, pore throats between 0–200 nm are dominant, accounting for 90% of the total pore throats. For illite/smectite mixed layer, pore throats between 0–200 nm account for nearly 80%, while pore throats between 200–500 nm only account for 15%. For illite, pore throats below 100 nm account for 80%, while pore throats in the range of 100–500 nm only account for 20%. For chlorite, most throats are below 200 nm (Fig. 5).

In order to further characterize the micro-nano pores of the clay minerals, four kinds of pore throat parameters were introduced, including the length of the major axis, length of the minor axis, shape factor, and concave-convex degrees. Moreover, the maximum, minimum and average values of the four parameters were counted.

In terms of the maximum length of the major axis of pore throats, kaolinite is the largest (up to about 5000 nm), illite and the illite/smectite mixed layer are the second, and chlorite is the smallest (about 2200 nm). Similarly, in terms of the minimum length of the major axis of pore throats, the illite/smectite mixed layer is the largest (up to about 5200 nm), chlorite and illite are the second, and kaolinite is the smallest (about 2800 nm). In terms of the average length of the major axis of the pore throats, the illite/smectite mixed layer, illite, and kaolinite are not much different, and chlorite is the smallest, which indicates that the pore ellipticity of chlorite is smaller (Fig. 6).

In terms of the maximum length of the minor axis of the pore throats, the illite/smectite mixed layer is the largest (up to about 3750 nm), illite is the second, and the kaolinite and chlorite are the smallest (about 1600 nm). The chlorite is the smallest in terms of the average length of the major axis of pore throats.

In terms of the maximum and minimum values of the shape factor of the pore throats, the pores of the four clay minerals are not much different. Illite is the largest, followed by chlorite, kaolinite and the illite/smectite mixed layer in order, indicating that the pore roundness of illite is the largest.

5 Discussion

5.1 Determination of the lower limit of static pore throat

When molecules of crude oil pass through pore throats, they will undoubtedly be affected by their size. If the total

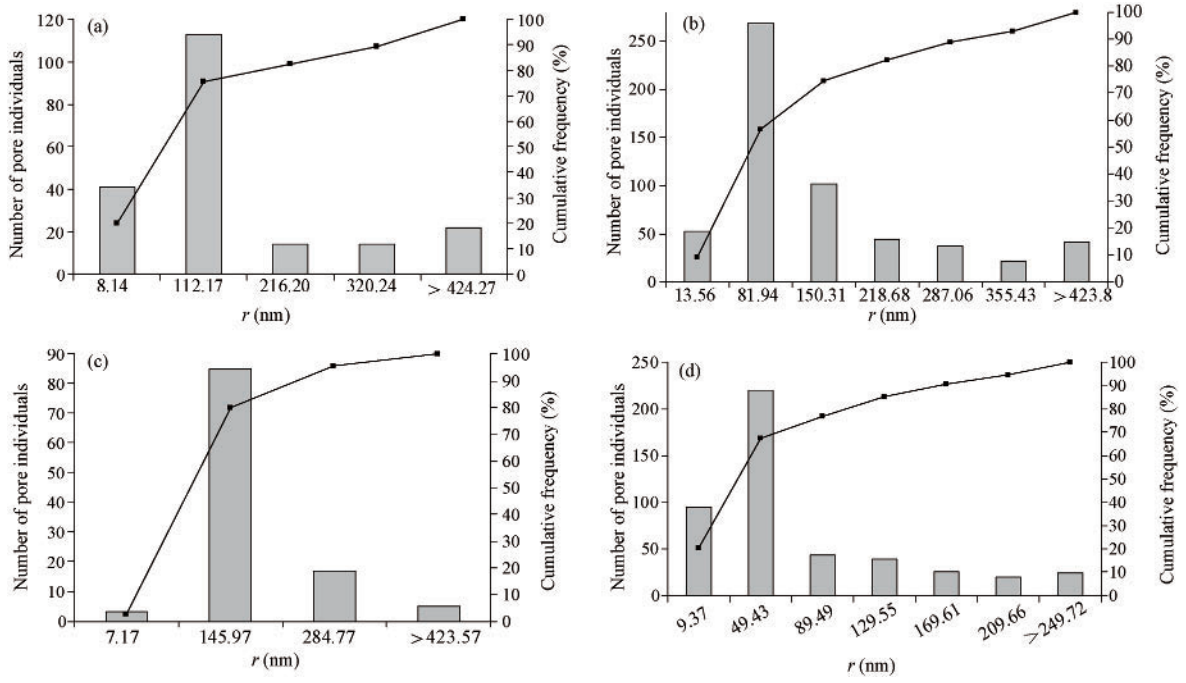

Fig. 5. Distribution graphs of the pore throat radius of four clay minerals
(a) kaolinite; (b) illite/smectite mixed layer; (c) illite; (d) chlorite.

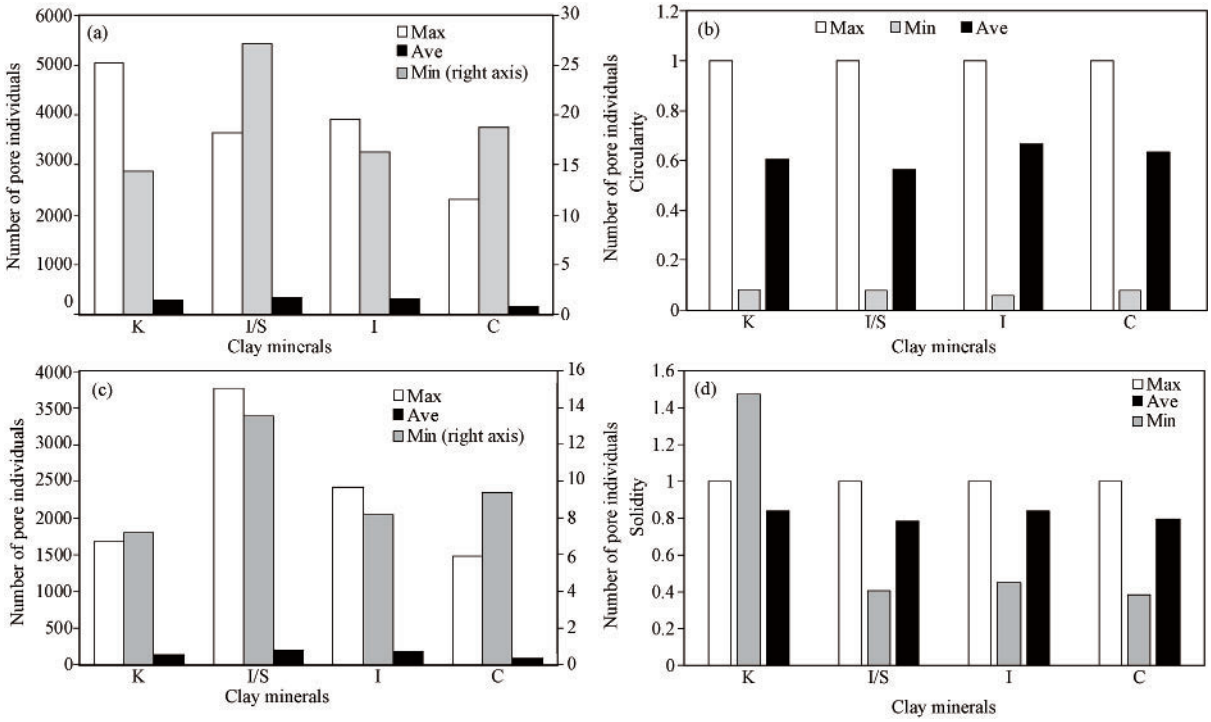

Fig. 6. Statistics of geometric characteristics of the micro-nano pore throats of clay minerals in the study area
(a) Major; (b) minor; (c) circularity; (d) solidity.

radius of the crude oil molecules is greater than the pore throat radius, it will be difficult or even impossible for the crude oil molecules to enter therein, not to mention the accumulation of oil and gas. From this point of view, not all nanopores play an important role in the reservoir permeability of oil and gas, that is, there is a certain reservoir threshold in the pore throat. Below this threshold, there will be little or no oil and gas accumulation and seepage activities, so researches on accumulation and seepage of that kind of reservoir are of less significance (Fig. 7). Therefore, in studies of storage of nanoscale, the pore size should not be required to reach several nanometers, while more attention should be paid to the development of storage above the lower limit of pore throats, in order to find the correct research direction of nanoscale reservoirs. The lower limit radius of the storage space of the Lower Karamay Fm. conglomerate reservoir was calculated by the method using the thickness of the bound water film and the molecular radius of crude oil. In the process of crude oil migration and reservoir formation, as with the capillary action and the adsorption of rock surface, it is impossible for oil to drive away all the water, some water remaining in the reservoir. Due to special distribution and state of existence, most of this water (irreducible water) is immobile, trapped in the corner of rock particle contact and in fine pores or adsorbed on the rock surface. According to the Hagen-Poiseuille equation (Huang et al., 1998), the thickness of the irreducible water can be calculated by Equation 1 (Zou et al., 2011):

$$d_i = \frac{714.2\phi S_{wi}}{A\rho} \quad (3)$$

where, d_i, the thickness of irreducible water, nm; 714.2,

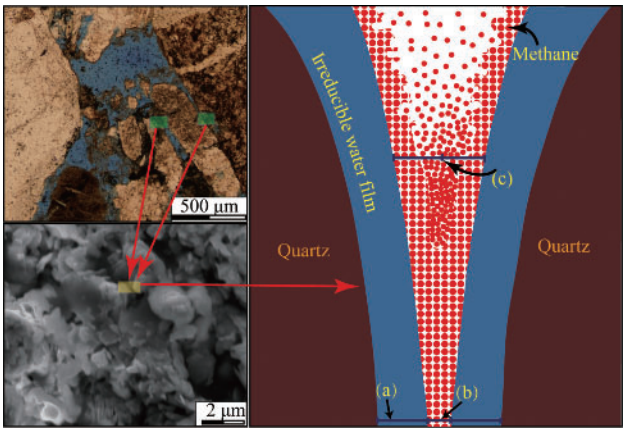

Fig. 7. Inferential model of the lower limit of physical properties of conglomerate reservoirs in Xinjiang (modified after Zou et al., 2011).

the conversion constant; φ, the core porosity (24%); S_{wi}, the bound water saturation (20.3%); A, the specific surface of rock (8.02 m^2/g); ρ, the core density (2.06 g/cm^3).

Among them, the values of the specific surface and the bound water saturation are the average values of multiple samples in the Lower Karamay Fm., and the average thickness of the bound water film (d_i) acquired by calculation is 21.064 nm. Therefore, the lower limit of the static pore throat radius is calculated to be 42.128 nm.

5.2 Determination of the lower limit of dynamic pore throat

Based on the mercury intrusion test data, this paper introduces the J Function (Zhang et al., 2004; Sun et al.,

2011), and uses the Purcell method to calculate the minimum flow pore throat radius. The calculation principle is as follows:

Firstly, using the *J* Function transformation on the capillary pressure, the average capillary pressure curve is constructed:

$$J(S_w) = \frac{p_c}{\sigma \cos\theta}\sqrt{\frac{K}{\phi}} \quad (4)$$

where, J, J Function, dimensionless; Pc, capillary pressure, MPa; σ, interfacial tension, mN/m; θ, wetting contact angle, °; K, permeability, 10^{-3} μm^2; φ, porosity, %; S_w—water saturation, %.

Since the contact occurs at the air-mercury interface during the mercury intrusion, the average capillary pressure curve is expressed as:

$$J(S_w) = 0.086 P_c \sqrt{\frac{K}{\phi}} \quad (5)$$

Purcell (1949) obtained the permeability contribution rate of a fixed pore throat radius by the relationship between the mercury injection pressure and the mercury inflow amount and accumulated the contribution rate. The pore throat radius with the cumulative permeability contribution rate of 99% is the minimum flow pore throat radius, that is, the lower limit of the dynamic pore throat. The principle is as follows:

$$\Delta K_{mi} = \frac{1}{2}\left(\frac{1}{P_{ci}^2} + \frac{1}{P_{ci+1}^2}\right)\cdot \Delta S_{i+1} \quad (6)$$

$$\Delta K_{mi} = \frac{\Delta K_{mi}}{\sum_{i-1}^{n} \Delta K_{mi}} \quad (7)$$

$$\sum_{i-1}^{n} \Delta K_{mi} = \Delta K_1 + \Delta K_2 + \ldots + \Delta K_n \quad (8)$$

where, ΔS_{i+1}, interval mercury inflow amount, %; ΔK_ir, permeability contribution rate of a fixed pore throat radius; $\Sigma^{n}_{i=1}\Delta K_i$, cumulative permeability contribution rate.

The lower limit of the dynamic pore throat calculated by the Purcell method is 72.42 nm, that is, the lower limit of the dynamic pore throat of the conglomerate reservoir with nano-scale pores is 72.42 nm. According to Laplace's equation of capillary pressure, the flow of fluids at the nanometer scale requires a large pressure difference, so the lower limit of the dynamic pore throat should be greater than the lower limit of the static pore throat. Combined with the lower limits of the dynamic and static pore throat, for tight oil reservoirs, pore throats below about 72.42 nm contribute little to the seepage of tight oil and formation water (Fig. 8).

5.3 Development mechanism of pore throats

As shown in Fig. 9, for the four types of minerals, the radius of the pore throats increases linearly with the increase of the length of the major axis and the minor axis of pore throats, and it shows two important characteristics. Firstly, when the length of the major axis and minor axis change in the same way, the change in the short axis would lead to a faster change in pore radius, which indicates that the increase of the short axis plays a greater role in promoting the growth of the pores. Secondly, when the length of the long axis and short axis of the pore throat are small, the linear relationship with the radius is strong. When the value is higher than a certain value, the linear relationship begins to weaken. This suggests that the length of the pore throat is not the only factor controlling pore growth. For the major and minor axes of pore throats, they complement each other.

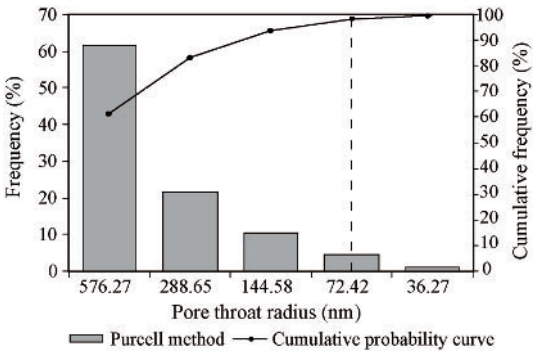

Fig. 8. Schematic diagram for calculating the lower limit of dynamic pore throat using the Purcell method.

For illite, the shape factor exhibits a nonlinear decrease with increasing pore radius and length of major and minor axes. This indicates that the larger the illite pores, the more easily the ellipticity increases, and the easier to form narrow pores.

5.4 Contribution of secondary pores of clay minerals to fluid storage and seepage

The clay minerals can be dissolved, broken and migrate under water injection. Under the drag and carry of the higher viscosity crude oil, the dissolved and broken materials are continuously taken out of formations, resulting in a major change in reservoir properties. The lower limit of the static pore throat of the secondary pore was calculated as 42.128 nm, and the lower limit of the dynamic pore throat was 72.42 nm. Different types of clay minerals differ in the contribution rate of storage and seepage in the study area. Gkay and Rex (1966) were first to study the formation damage, and concluded that the migration of smectite, illite and kaolinite particles in the formation water could plug the pore throats and decrease permeability. Baker et al. (1993) by using ESEM microscopy directly observed that water intrusion would affect the illite/smectite mixed layer and lead to the formation of highly permeable swelling gel smectite (80–90%). In the study area, the illite/smectite mixed layer is more water sensitive than other three minerals. Illite/smectite mixed layer will expand dozens of times after contacting water, then the porosity is blocked, the permeability is significantly reduced, and the water sensitivity of the particle expansion is more serious than that of particle migration (Wang et al., 2019).

Kaolinite has the highest content in the clay minerals in the study area, and is mainly sheet-like. The sheet-like sedimentary pores have a greater binding effect on crude oil, and it is difficult to drive oil out of the pores.

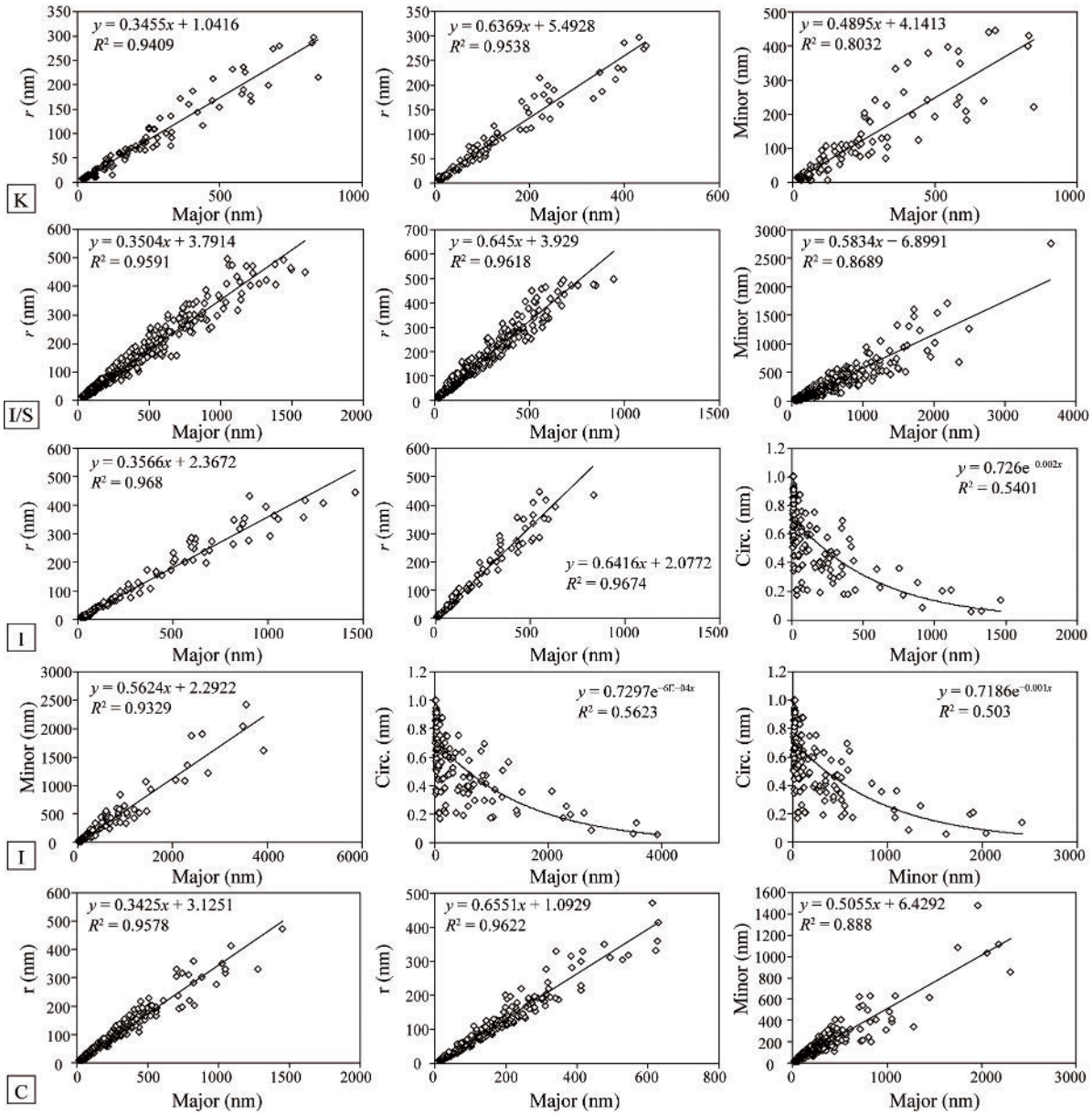

Fig. 9. Correlation analysis of the attribute parameters of pore throats.
K, kaolinite; I/S, illite/smectite mixed layer; I, illite; C, chlorite

Therefore, the contribution rate to the storage of kaolinite in the study area is 52.72%. The sheet-like kaolinite is converted to dickite or metahalloysite, resulting in disintegration, fragmentation and volume increase of kaolinite minerals in the same pores, and the permeability is greatly reduced (Hayatdavoudi and Ghalambor, 1996, 1998). It was observed that kaolinite was converted to illite (brammallite) in 75–15 days in highly alkaline potassium hydroxide solutions (pH >11) at 35°C and 80°C (Bauer et al., 1998). In addition, there are macro-pores, and even meso-pores (2–50 nm) and micro-pores (<2 nm) in the kaolinite aggregates in the clastic rocks (IUPAC). The surface of the kaolinite has two types, Si-O surface and Al-OH surface (Tunega et al., 2002). Therefore, the octahedral and tetrahedral surfaces of kaolinite have different chemical properties, which are considered hydrophilic and hydrophobic (Tunega et al., 2004; Niu and Qiang, 2009). The silica surface of kaolinite is oleophilic to some extent, whereas the hydroxyl surface is completely hydrophilic. NaCl in the pore fluid affects the wettability of kaolinite and changes the wettability of the silica surface of kaolinite to completely hydrophilic. All kaolin minerals have a small amount of permanent negative charge and a low cation exchange capacity, and can easily form an oil film on the surface with the nature of oleophilic or weak oleophilic (Wilson et al., 2014b). The larger the exchange amount of the cation, the more the charge on the surface of clay minerals, and the larger the adsorption amount because of the charge attraction of polymer, surfactant and alkali. Therefore, the contribution rate of kaolinite to seepage in the study area is only 38.18%.

In the sections where illite/smectite and kaolinite are rich in the study area, the most significant effect on the saturation of mobile fluid is the reduction of water absorption capacity of the reservoir because the hydration and swelling of smectite can block pores in the reservoirs. Smectite and illite flakes generally arise in the form of silk- or skirt-like or locally occur as cellular, forming large amounts of circular pores (Fig. 4). Locally enlarged images show that smectite particles of petal shape are crosswise arranged and larger pores form in the center of intersection regions. The maximum pore diameter is 12.9 μm, the minimum value is 0.36 μm, and the average value is 3.55 μm. Therefore, the contribution of illite/smectite to the storage capacity in all the clay minerals is estimated to be 60%, and its contribution to flow capacity is also significant (45.86%). Due to the strong water sensitivity of the illite/smectite mixed layer, the actual contribution rate is slightly smaller than the above values.

Flaky, filamentous and curved illite within interparticle pores or on the surface of mineral grains segments the original larger pore into numerous smaller pores. As a result, the flow channel of the fluid becomes tortuous and the permeability is significantly reduced. Under the effect of formation water, much more illite migrates than kaolinite (Wilson et al., 2104a). At proper hydrodynamic conditions, authigenic clay (such as stripped illite) in the fluid separates, disperses, migrates and precipitates in the throats, blocking fluid and reducing permeability (Wilson et al., 2014b). Thin layers of illite coating the surface of pores and filamentous illite increase the surface area, and irreducible water proportion and decrease the effective pore radius of the core samples, which is the reason that its contribution rate to total storage is 37.07% in the study area (Fig. 10a). In addition, hair-like illite further promotes the surface area and roughness of pores. For the oil adsorbed on the irregular surface of pores, consequently, only oil in the centers of pores are motivated during water flooding process. In the study area, therefore, the contribution rate of illite to the total flow capacity is as low as 28.78% (Fig. 10b). Due to the strong water sensitivity of the illite, the actual contribution rate is slightly smaller than the above values.

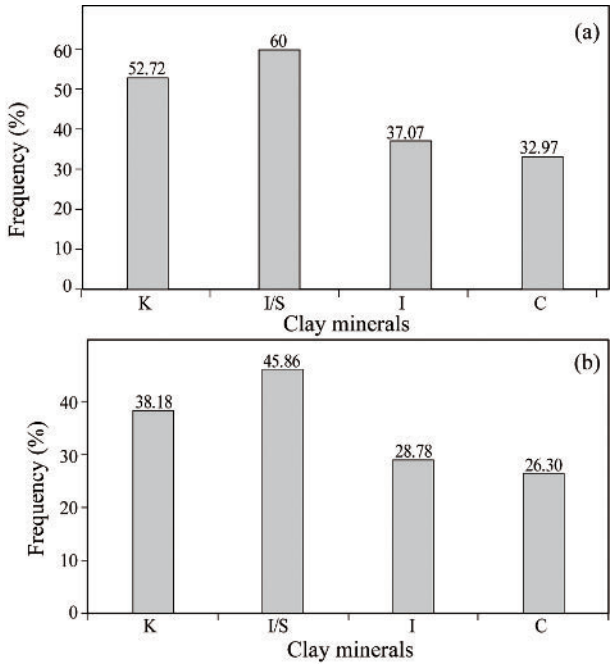

Fig. 10. Contribution rate of secondary pores to storage space (a) and seepage (b) in the study area (symbols see Fig. 7).

As for chlorite in the study area, triangle pores exist between particle assemblages and several slit-like pores were found between flakes in local areas. Its contribution rate to storage is 32.97%. Due to the bridge structure of the chlorite within pores, it has a negative effect on flow capacity, then the contribution rate is 26.3%.

6 Conclusions

We have studied the pore-structure characterization of clay minerals in the Triassic Lower Karamay Fm. conglomerate reservoir in the Junggar Basin and its impact on hydrocarbon storage and seepage.

A conglomerate reservoir is a very special kind of reservoir. The comprehensive characteristics of the pores of clay minerals in this kind of reservoir have seldom been paid attention to before, but our research shows that this is very necessary.

For the different types of clay minerals found in our study, there are clear differences in content, geometric shape and distribution characteristics of the secondary pores, which are mainly manifested in pore radius, long axis length and short axis length. The minimum radius of the static pore throat and the minimum radius of fluid flow in the conglomerate reservoir are also given by combining theoretical model with experimental measurement. Therefore, the pore development characteristics of different types of clay minerals will play different roles in oil and gas storage and seepage. This is of great significance for us to better understand the conglomerate reservoir.

The lower limits of the dynamic and static pore throat radius are 42.128 nm and 72.42 nm, respectively. The theoretical contribution rates of illite/smectite mixed layer, kaolinite, illite and chlorite of storage (seepage) are 60% (45.86%), 52.72% (38.18%), 37.07% (28.78%) and 32.97% (26.3%), respectively.

More work is still needed on the visualization of fluid flow in clay minerals. In this way, our research outcomes can be used more quickly in the effective development of conglomerate oil and gas, to realize its due industrial value.

Acknowledgements

This work is granted by PetroChina Innovation Foundation (Grant No. 2019D-5007-0214) and the National Mega Project of Oil and Gas (Grant No. 2017ZX05013005-009). As well as grateful to Susan Turner (Brisbane) assisted with English language.

Manuscript received Dec. 11, 2018
accepted Feb. 02, 2019

associate EIC: SHU Degan
edited by GUO Xianqing

References

Arnott, R.W.C., 2003. The role of fluid- and sediment-gravity flow processes during deposition of deltaic conglomerates (Cardium Formation, Upper Cretaceous), west–central Alberta. Bulletin of Canadian Petroleum Geology, 51(4): 426–436.

Baker, J.C., Uwins, P.J.R., and Mackinnon, I.D.R., 1993. ESEM study of illite/smectite freshwater sensitivity in sandstone reservoirs. Journal of Petroleum Science & Engineering, 9(2): 83–94.

Bauer, A., Velde, B., and Berger, G., 1998. Kaolinite transformation in high molar KOH solutions. Applied Geochemistry, 13(5): 619–629.

Carvalho, A.D.S.G., and Ros, L.F.D., 2015. Diagenesis of Aptian sandstones and conglomerates of the Campos Basin. Journal of Petroleum Science and Engineering, 125: 189–200.

Cerepi, A., Durand, C., and Brosse, E., 2002. Pore microgeometry analysis in low-resistivity sandstone reservoirs. Journal of Petroleum Science and Engineering, 35 (3–4): 205–232.

Chen, S., Han, Y., Fu, C., Zhu, Y., and Zuo, Z., 2016. Micro and nano-size pores of clay minerals in shale reservoirs: Implication for the accumulation of shale gas. Sedimentary Geology, 342: 180–190.

Clarke, R.H., 1979. Reservoir properties of conglomerates and conglomeratic sandstones: Geological notes. AAPG Bulletin, 63(5): 799–803.

Clifton, H.E., 2003. Supply, segregation, successions, and significance of shallow marine conglomeratic deposits. Bulletin of Canadian Petroleum Geology, 51(4): 370–388.

Curtis, M.E., Cardott, B.J., Sondergeld, C.H., and Rai, C.S., 2012. Development of organic porosity in the Woodford Shale with increasing thermal maturity. International Journal of Coal Geology, 103: 26–31.

Feng, X., Peng, X., Li, L., Yang, X., Wang, J., Li, Q., Zhang, C. and Deng, H., 2019. Influence of reservoir heterogeneity on water invasion differentiation in carbonate gas reservoirs. Natural Gas Industry B, 6(1): 7–15.

Gkay, D. H., and Rex, R. W., 1966. Formation damage in sandstones caused by clay dispersion and migration. Clays and Clay Minerals, 14(1): 355–362.

Hart, B.S., and Plint, A.G., 2003. Stratigraphy and sedimentology of shoreface and fluvial conglomerates: Insights from the Cardium Formation in NW Alberta and adjacent British Columbia. Bulletin of Canadian Petroleum Geology, 51(4): 437–464.

Hayatdavoudi, A., and Ghalambor, A., 1996. Controlling formation damage caused by kaolinite clay minerals: Part I. SPE formation damage control symposium. Society of Petroleum Engineers, SPE, 31118: 473–479.

Hayatdavoudi, A., and Ghalambor, A., 1998. Controlling formation damage caused by kaolinite clay minerals: PartII. SPE formation damage control symposium. Society of Petroleum Engineers, SPE, 39464: 421–430.

He, M., Jin, Z., Li, T., Guo, X., and Yang, T., 2014. Stratigraphic framework and microfacies of the Triassic Lower Karamay Formation in districts I, III, NW Junggar, China. Journal of Earth Science, 25(6): 1003–1017.

Hu, Z., Mu, Y., Gu, Z., Duan, X. and Li, Y., 2020. Law of imbibition effect on shale gas occurrence state. Natural Gas Industry B, 7(6): 624–630.

Huang, P., Xu, N.P., and Shi, J., 1998. Pore size distribution determination of inorganic members by liquid-liquid displacement porometry. Journal of Nanjing of Chemical Technology, 20(3): 45–50 (in Chinese with English Abstract).

Hurst, A., 1999. Textural and geochemical micro-analysis in the interpretation of clay mineral characteristics: Lessons from sandstone hydrocarbon reservoirs. Clay Minerals, 34(1): 137–137.

Jia, H., Ji, H., Wang, L., Gao, Y., Li, X., and Zhou, H., 2017. Reservoir quality variations within a conglomeratic fan-delta system in the Mahu Sag, northwestern Junggar Basin: Characteristics and controlling factors. Journal of Petroleum Science and Engineering, 152: 165–181.

Kuila. U., McCarty, D.K., Derkowski, A., Fischer, T.B., Topor, T., and Prasad, M., 2014. Nano-scale texture and porosity of organic matter and clay minerals in organic-rich mudrocks. Fuel, 135: 359–373.

Lai, J., Wang, G.W., Chen, M., Wang, S.A., Chai, Y., Cai, C., Zhang, Y.C., and Li, J.L., 2013. Pore structures evaluation of low permeability clastic reservoirs based on petrophysical facies: A case study on Chang 8 reservoir in the Jiyuan region, Ordos Basin. Petroleum Exploration and Development, 40(5): 566–573 (in Chinese with English Abstract).

Li, Y., Li, S.T., Mou, W.W., and Yan, C.C., 2017. Influences of clay minerals on physical properties of Chang 6 tight sandstone reservoir in Jiyuan area, Ordos Basin. Natural Gas Geoscience, 28(7): 1043–1053 (in Chinese with English Abstract).

Li, J.Z., Yan, K., Ren, H.Q., and Sun, Z.F., 2020. Detailed quantitative description of fluvial reservoirs: A case study of L6-3 layer of sandgroup 6 in the second member of Shahejie Formation, Shengtuo Oilfield, China. Advances in Geo-Energy Research, 4(1): 43–53.

Liu, H., Jiang, Z., Zhang, R., and Zhou, H., 2012. Gravels in the Daxing conglomerate and their effect on reservoirs in the Oligocene Langgu Depression of the Bohai Bay Basin, North China. Marine and Petroleum Geology, 29(1): 192–203.

Liu, J.K., 1983. An investigation on structure model of conglomeratic reservoir and its evaluation. Petroleum Exploration and Development, 10(2): 45–56 (in Chinese with English Abstract).

Liu, Y., Xian, C.G., Li, Z., Wang, J.G., and Ren, F., 2020. A new classification system of lithic-rich tight sandstone and its application to diagnosis high-quality reservoirs. Advances in Geo-Energy Research, 4(3): 286-295.

Liu, Z., Gao, B., Feng, D., Cui, X., Du, W., Wang, Y. and Li, D., 2017. Mineral composition of the Lower Cambrian black shale in the Upper Yangtze region and its significance in oil and gas exploration. Natural Gas Industry B, 4(5): 340-345.

Luo, M.G., and Zhang, T.H., 1992. Micropore structure and classification of conglomerate reservoir formation in Karamay Oilfield. Oil and Gas Geology, 13(2): 201–210 (in Chinese with English Abstract).

Lv, J.R., Tan, F.Q., Xu, C.F., Sun, N., Zhou, Y.Z., and Fu, W.Q., 2015. Reservoir classification characteristics and water displaced oil laws of conglomerate reservoir in Karamay Oilfield. Journal of Northeast Petroleum University, 39(4): 21–30 (in Chinese with English Abstract).

Mahmic, O., Dypvik, H., and Hammer, E., 2018. Diagenetic influence on reservoir quality evolution, examples from Triassic conglomerates/arenites in the Edvard Grieg field, Norwegian North Sea. Marine and Petroleum Geology, 93: 247–271.

Mohammadi, M.R., Bahmaninia, H., Ansari, S., Hemmati-Sarapardeh, A., Norouzi-Apourvari, S., Schaffie, M. and Ranjbar, M., 2021. Evaluation of asphaltene adsorption on minerals of dolomite and sandstone formations in two and three-phase systems. Advances in Geo-Energy Research, 5(1): 39–52.

Morad, S., Ketzer, J.M., and Ros, L.F.D., 2010. Spatial and temporal distribution of diagenetic alterations in siliciclastic rocks: Implications for mass transfer in sedimentary basins. Sedimentology, 47(s1): 95–120.

Nelson, P.H., 2009. Pore-throat sizes in sandstones, tight sandstones, and shales. AAPG Bulletin, 93(3): 329–340.

Niu, J.N., and Qiang, Y.H., 2009. Molecular dynamics simulation on structure of water molecules in a kaolinite-water system. Acta Physico-Chimica Sinica, 25(06): 1167–1172 (in Chinese with English Abstract).

Pan, J., Zhang, Z.Z., Li, M., Wu, Y.W. and Wang, K., 2019. Characteristics of multi-scale pore structure of coal and its influence on permeability. Natural Gas Industry B, 6(4): 357-365.

Purcell, W.R., 1949. Capillary pressures-their measurement using mercury and the calculation of permeability therefrom.

Journal of Petroleum Technology, 1(2): 39–48.
Rafiei, Y. and Motie, M., 2019. Improved reservoir characterization by employing hydraulic flow unit classification in one of Iranian carbonate reservoirs. Advances in Geo-Energy Research, 3(3): 277–286.
Rogers, J.P., 2007. New reservoir model from an old oil field: Garfield conglomerate pool, Pawnee County, Kansas. AAPG Bulletin, 91(10): 1349–1365.
Rong, H. and Bai, H., 2014. Pore structure characteristics of the relative water-resisting layer on the top of the Ordovician in Longgu Coal Mine. International Journal of Mining Science and Technology, 24(5): 657–661.
Sakthivel, S., and Venkatesh, R. P., 2012. Solid state synthesis of nano-mineral particles. International Journal of Mining Science and Technology, 22(5): 651–655.
Salem, A.M., Morad, S., Mato, L.F., and Al-Aasm, I.S., 2000. Diagenesis and reservoir-quality evolution of fluvial sandstones during progressive burial and uplift: Evidence from the Upper Jurassic Boipeba Member, Recôncavo Basin, Northeastern Brazil. AAPG Bulletin, 84(7): 1015–1040.
Song, Z.Q., Sun, Y., Chang, L., Wei, J.K., and Yang, H.G., 2009. Characteristics and remaining oil distribution of heterogeneous conglomerate reservoir in Karamay Oilfield. Fault-Block Oil and Gas Oilfield, 6: 54–58 (in Chinese with English Abstract).
Song, Z.Q., Yang, L.L., Cheng, Y., Wang, N., and Ding, J., 2007. Comprehensive evaluation of heterogeneity conglomerate reservoir-taking conglomerate reservoirs in Qizhong and Qidong area of Karamay oilfield as an example. Petroleum Geology and Experiment, 29(4): 415–419 (in Chinese with English Abstract).
Su, R.N., Lu, A.H., Liu, Z.R., and Wang, C.Q., 2007. An experimental study of neutral modification of montmorillonite. Acta Petrologica et Mineralogica, 26(6): 505 –510 (in Chinese with English Abstract).
Sun, J.C., Yang, Z.M., and Xiao, Q.H., 2011. The history of constant-Rate mercury injection technology and its application on the development of petroleum fields. Advances in Porous Flow, 01(1): 1–7 (in Chinese with English Abstract).
Taylor, T.R., Giles, M.R., Hathon, L.A., Diggs, T.N., Braunsdorf, N.R., Birbiglia G.V., Kittridge, M.G., Macaulay, C.I., and Espejo I.S., 2010. Sandstone diagenesis and reservoir quality prediction: Models, myths, and reality. AAPG Bulletin, 94(8): 1093–1132.
Tunega, D., Haberhauer, G., Gerzabek, M.H., and Lischka, H., 2002. Theoretical study of adsorption sites on the (001) surfaces of 1:1 clay minerals. Langmuir, 8(1): 139–147.
Tunega, D., Gerzabek, M.H., Lischka, H., 2004. Ab initio molecular dynamics study of a monomolecular water layer on octahedral and tetrahedral kaolinite surfaces. The Journal of Physical Chemistry B, 108(19): 5930–5936.
Wang, B., Qin, Y., Shen, J., Wang, G., Zhang, Q., and Liu, M., 2019. Experimental study on water sensitivity and salt sensitivity of lignite reservoir under different pH. Journal of Petroleum Science and Engineering, 172: 1202–1214.
Wei, W., Zhu, X., Tan, M., Xue, M., Guo, D., Su, H., and Wang, P., 2015. Diagenetic and porosity evolution of conglomerate sandstones in Bayingebi Formation of the Lower Cretaceous, Chagan Sag, China-Mongolia frontier area. Marine and Petroleum Geology, 66: 998–1012.
Wilson, L., Wilson, M.J., Green, J., and Patey, I., 2014b. The influence of clay mineralogy on formation damage in North Sea reservoir sandstones: A review with illustrative examples. Earth-Science Reviews, 134: 70–80.
Wilson, M.J., Wilson, L., and Patey, I., 2014a. The influence of individual clay minerals on formation damage of reservoir sandstones: A critical review with some new insights. Clay Minerals, 49(2): 147–164.
Xiao, M., Yuan, X.J., Wu, S.T., Cao, Z.L., Tang, Y., Xie, Z.R., and Wang, R.J., 2019. Conglomerate reservoir characteristics of and main controlling factors for the Baikouquan Formation, Mahu Sag, Junggar Basin. Earth Science Frontiers, 26(1): 1–13 (in Chinese with English Abstract).
Xie, Z.Y., Wei, G.Q., Zhang, J., Yang, W., Zhang, L., Wang, Z.H., and Zhao, J., 2017. Characteristics of source rocks of the Datangpo Fm, Nanhua System, at the southeastern margin of Sichuan Basin and their significance to oil and gas exploration. Natural Gas Industry B, 4(6): 405–414 (in Chinese with English Abstract).
Yang, B., Qu, H.J., Pu, R.H., Tian, X.H., Yang, H., Dong, W.W., and Chen, Y.H., 2020. Controlling effects of tight reservoir micropore structures on seepage ability: A case study of the Upper Paleozoic of the eastern Ordos Basin, china. Acta Geologica Sinica (English Edition), 94(2): 322–336.
Yao, S., Jiao, K., Li, M., and Wang, H., 2012. Advances in research of coal and kerogen nanostructure. Advances in Earth Science, 27(4): 367–378.
Yin, S.L., Chen, G.Y., Chen, Y.K., and Wu, X.J., 2018. Control effect of pore structure modality on remaining oil in glutenite reservoir: A case from Lower Karamay Formation in block Qidong 1 of Karamay Oilfield. Lithologic Reservoirs, 30(05): 91–102 (in Chinese with English Abstract).
Zeng, Y.J., Du, S.H, Zhang, X., Zhang, B.P., and Liu, H.L., 2020. The crucial geometric distinctions of microfractures as the indispensable transportation channels in hydrocarbon-rich shale reservoir. Energy Reports, 6: 2056–2065.
Zhang, D.Y., Peng, Y.C., Xiao, F.W., Shi, Y.L., and Yao, M., 2013. Pore structure and influence factors of conglomerate reservoir — Case study of lower Karamay formation in mid and east of 7th block, Karamay oilfield. Petroleum Geology and Recovery Efficiency, 20(6): 29–34 (in Chinese with English Abstract).
Zhang, S.Q., Xie, L., Yang, B.Y., Xu, F., and Ma, J., 2004. Application of minimum flow pore throat radius method to determine the lower limit of Physical properties in Yeshaishan Oilfield. Qinghai Petroleum, 4: 44–46 (in Chinese).
Zou, C.N, Zhu, R.K, Bai, B., Yang, Z., Wu, S.T., Su, L., Dong, D.Z., and Li, X.J., 2011. First discovery of nano-pore throat in oil and gas reservoir in China and its scientific value. Acta Petrologica Sinica, 27(6): 1857–1864 (in Chinese with English Abstract).

About the first author

Taskyn ABITKAZY, Male, from Kazakhstan, born in 1985; Ph.D., graduated from Peking University. He is now engaged in oil-gas field development at the Research Institute of Petroleum Exploration and Development, CNPC, Beijing. Email: taskyn@pku.edu.cn. phone: 010-83595090.

About the corresponding author

DU Shuheng is an assistant professor at State Key Laboratory of Nonlinear Mechanics, Institute of Mechanics, Chinese Academy of Sciences. He received his B.A. at the China University of Geosciences in 2013 and Ph.D. in Peking University in 2018. He is a member of the first young editorial board of the Chinese journal *Natural Gas Industry*. His current research interest is focused on unconventional hydrocarbon geology and mechanics. Email: dushuheng@imech.ac. cn.